Connecting Shock Velocities to Electron-Injection Mechanisms

M. E. Dieckmann,[1,*] B. Eliasson,[2,†] A. Stathopoulos,[3,‡] and A. Ynnerman[1,§]
[1]*ITN, Linköpings University, 60174 Norrköping, Sweden*
[2]*Theoretische Physik IV, Ruhr-Universität Bochum, D-44780 Bochum, Germany*
[3]*Department of Computer Science, College of William and Mary, Williamsburg, Virginia 23187-8795, USA*
(Received 24 June 2003; revised manuscript received 19 September 2003; published 13 February 2004)

Electrons can be accelerated by their interaction with nonlinearly saturated electrostatic waves up to speeds with which they can undergo diffusive acceleration across supernova remnant shocks. Here, we model this wave-electron interaction by particle-in-cell and Vlasov simulations. We find that the lifetime of the saturated wave is considerably longer in the Vlasov simulation, due to differences in how these simulation methods approximate the plasma. Electron surfing acceleration which requires a stable saturated wave may thus be more important for electron acceleration at shocks than previously thought. For beam speeds above a critical value, which we estimate here, both simulation codes exclude surfing acceleration due to a rapid wave collapse.

DOI: 10.1103/PhysRevLett.92.065006 PACS numbers: 52.65.Rr, 52.35.Fp, 52.65.Ff, 98.70.Sa

Supernova remnant (SNR) shocks are believed to be a major source of cosmic rays in the galaxy [1]. Synchrotron emission indicates the presence of highly relativistic electrons [1,2] which are likely to be produced by diffusive shock acceleration [3–5]. To undergo diffusive shock acceleration, electrons must cross the shock repeatedly. The orientation of the shock normal relative to the magnetic field $\boldsymbol{B}$ sets the conditions electrons need to fulfill to be accelerated. Shocks for which the shock normal is orthogonal to $\boldsymbol{B}$ are believed to be most efficient for electron acceleration [5]. The thickness of such shocks is comparable to the ion Larmor radius. To undergo diffusive acceleration, the electrons must have Larmor radii exceeding the shock thickness. This implies electron energies of 10^5 eV or more which significantly exceeds the 10 eV of the cool interstellar medium (ISM) and the 10^2 eV of the hot ISM [4,5]. The electrons must thus be preaccelerated.

The interaction between electrostatic waves and the electrons is a candidate mechanism for their preacceleration or injection and recently evidence from particle-in-cell (PIC) simulations confirming that idea has been brought forward [6–12]. Here we use the simple model [6–8] shown in Fig. 1. The shock-reflected ion beams in this model excite electrostatic waves which saturate by trapping electrons. Stable Bernstein-Greene-Kruskal (BGK) modes [13] should develop but the previous work in [6–8] has shown that the sideband instability limits the lifetime of the BGK mode. For realistic beam speeds of $v_b/c \approx 0.06$ we found in [7] that the BGK mode collapse could accelerate electrons up to 1.5×10^4 eV which is less than the required 10^5 eV for electron injection. Excluding the sideband instability increases the lifetime of the BGK mode. Then the transport of trapped electrons across $\boldsymbol{B}$ accelerates electrons up to 6×10^4 eV [7] and above [9,10].

The previous studies in [6–12] have not addressed how the stability of the BGK mode depends on the numerical scheme and on the BGK mode speed. Here we compare the result computed by a PIC simulation [8] with the results from Vlasov simulations for two BGK mode speeds. In what follows we set ω_p, n_0, $v_{\mathrm{th},j}$, and ϵ_0 to be the plasma frequency, the electron density, and the thermal velocity $(k_B T_j/m_j)^{0.5}$ of each of the j particle species with their initially Maxwellian velocity distribution and the dielectric constant. The index j equals e, bp, $b1$, and $b2$ for the electrons, the bulk protons, and both beams. We use the proton to electron mass ratio $m_p/m_e = 1830$ for all three proton species. We use q_j to denote the charge of species j and e is the proton charge.

The primed variables $x = v_{\mathrm{th},e}\omega_p^{-1}x'$, $t = \omega_p^{-1}t'$, $v = v_{\mathrm{th},e}v'$, $f_j = n_0 v_{\mathrm{th},e}^{-1} f_j'$, and $E = v_{\mathrm{th},e}\sqrt{n_0 m_e/\epsilon_0}E'$ are dimensionless. Our simulations solve the Vlasov-Maxwell equations in 1D for an unmagnetized plasma, given by the

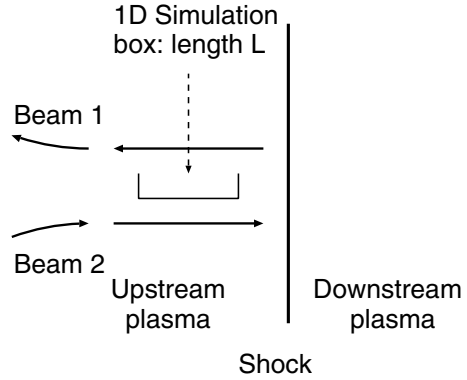

FIG. 1. The shock reflects a fraction of the upstream ions. These form beam 1 which, after being rotated by the upstream magnetic field, returns to the shock as beam 2. By placing our simulation box close to the shock and by ignoring the fact that the beam cannot rotate by a full π due to the shock motion we can model injection by a one-dimensional model where we place two counterpropagating ion beams in the upstream plasma.

equations describing the phase space density evolution for the four particle species in Eq. (1) and the evolution equation for the electrostatic field in Eq. (2). The PIC code solves them by the method of characteristics; the Vlasov code directly [14–16]:

$$\frac{\partial f_j'}{\partial t'} + v' \frac{\partial f_j'}{\partial x'} + \frac{q_j m_e}{e m_j} E' \frac{\partial f_j'}{\partial v'} = 0, \tag{1}$$

$$\frac{\partial E'}{\partial x'} = \sum_i \int f_i'(x', (v' - \hat{v}_i'), t') dv' - \int f_e'(x', v', t') dv'. \tag{2}$$

The summation over i in Eq. (2) is over bp, $b1$, and $b2$. The relative densities of the proton species are $n_i' = n_i/n_0$, where $n_0 = \sum_i n_i$. We set $n_{b1}' = n_{b2}' = 1/6$. Their mean velocities are $\hat{v}_i'$. We perform two Vlasov simulations with different beam velocities. We refer to the simulation with $\hat{v}_{b1}' = -\hat{v}_{b2}' = 21$ as case 1 and the simulation with $\hat{v}_{b1}' = -\hat{v}_{b2}' = 15$ as case 2. In the PIC simulation (case 3) we set $\hat{v}_{b1}' = -\hat{v}_{b2}' = 15$ as in [8]. We will use these cases as labels in the text and in the figures. The temperatures T_{bp}, T_{b1}, and T_{b2} are those of the bulk protons and the beams 1 and 2. They are set to $T_{b1} = T_{bp} = 10 \times T_e$ and $T_{b2} = 100 \times T_e$, where T_e is the electron temperature. We set $T_{bp} > T_e$ to suppress strong turbulence as discussed in [8] and $T_{b2} > T_{b1}$ to suppress the growth of a wave by $b2$, allowing us to focus on a single BGK mode. We leave the discussion of a system with two waves to future work.

Our simulations use periodic boundary conditions in space. The box length of $L = 8\pi v_{b1}/\omega_p$ is represented by 800 grid cells. The PIC simulation uses 6144 particles per cell (ppc) for the electrons and 2400 ppc for each of the proton species. The Vlasov simulations resolve phase space with a velocity step size $dv = 0.1 \times v_{\mathrm{th},e}$ up to the maximum velocity $|v_{\max}| = 100 \times v_{\mathrm{th},e}$.

A plasma with the parameters above is unstable and an electrostatic wave grows. The most unstable wave has a frequency ω_u that is slightly below ω_p. The most unstable wave number k_u fulfills the condition $\omega_u/k_u \approx \hat{v}_{b1}$. As we have found in [8] the wave saturates by electron trapping. The maximum velocity width v_T of the island in which an electron is trapped by a wave with a constant electric field amplitude E_T is obtained from $E_T = v_T^2 m_e k_u/4e$. Since $\omega_u/k_u \gg v_{\mathrm{th},e}$ no electron is initially trapped by the wave. The wave saturates once the separatrix of the trapped particle island reaches the electron thermal population. We obtain an estimate $E_T = E_c$ for this critical field by setting the width of the trapped particle island to the phase velocity of the wave times a factor that approximates the change in the mean speed of the thermal electrons by the wave potential, giving the condition $v_T = \sqrt{2}\omega_u/k_u$. By using $\omega_p \approx k_u \hat{v}_{b1}$ we obtain $E_c' = \hat{v}_{b1}'/2$ in dimensionless variables.

In Fig. 2 we show the time evolution of the waves driven by $b1$ in both Vlasov simulations and in the PIC simulation.

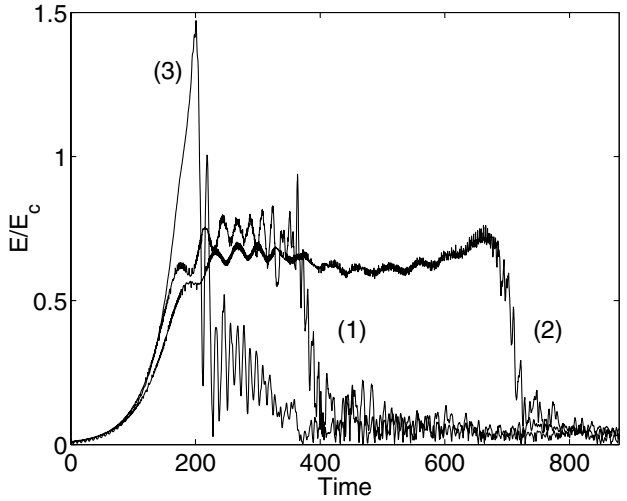

FIG. 2. The figure shows $E(t')/E_c$ for the waves driven by $b1$ in the three simulations. The labels (1), (2), and (3) correspond to the Vlasov simulation with the fast beam, the slow beam, and the PIC simulation, respectively. All waves initially grow exponentially, they then saturate, and finally they collapse. The peak amplitude and the time interval between saturation and collapse depend on $\hat{v}_{b1}$ and on the numerical scheme.

The curves 1 and 3 show a comparable growth rate. Curve 2 shows a slower growth despite having the same plasma parameters as curve 3. In the frame of reference moving with $\hat{v}_{b1}$ we have a phase velocity $v_{\mathrm{ph},b1} = \omega_u/k_u - \hat{v}_{b1} \approx (\omega_u - \omega_p)/k_u$. We measure values of $v_{\mathrm{ph},b1}/v_{\mathrm{th},b1} \approx -3$ for all simulations. The accuracy is low due to the limited frequency resolution caused by the rapid wave growth.

The Vlasov simulations represent the proton beam density down to numerical roundoff covering the speed interval between $\pm 8 v_{\mathrm{th},b1}$ in the frame of reference moving with $\hat{v}_{b1}$. Therefore $v_{\mathrm{ph},b1}$ is in a velocity interval that is well resolved by the beam protons. By increasing the beam speed $\hat{v}_{b1}/v_{\mathrm{th},b1}$ in the Vlasov simulations, we reach the limit of a cold proton beam. This may explain the faster growth of curve 1 compared to curve 2. For the PIC simulation the beam protons are well resolved in the frame of reference moving with $\hat{v}_{b1}$ within the limits $\pm 3 v_{\mathrm{th},b1}$ and here the phase speed $v_{\mathrm{ph},b1}$ is practically outside this velocity interval. As a consequence only the Vlasov code allows the beam ions to interact with the phase speed of the wave. The slowed wave growth of curve 2 compared to curve 3 despite that they both represent the same initial plasma parameters may thus be connected to Landau damping. We leave a more detailed investigation of this issue to future work.

The curves 1 and 2 in Fig. 2 saturate at $E/E_c \approx 0.7$ while curve 3 saturates at $E/E_c \approx 1.5$. The latter rapidly collapses as in [8]. This is in contrast to curves 1 and 2. We further notice from Fig. 2 that the lifetime of the BGK mode associated with curve 2 is longer than that of curve 1 indicating that the BGK mode stability increases for decreasing $\hat{v}_{b1}'$. Going from $\hat{v}_{b1}' = 21$ to $\hat{v}_{b1}' = 15$

increases the lifetime of the BGK mode to that in [7] where we suppressed the sideband instability and achieved substantial electron (surfing) acceleration due to the transport of trapped electrons across $\boldsymbol{B}$. By crossing this beam velocity interval, the lifetime of the BGK mode goes from being limited by the sideband instability to being limited by the absorption of wave energy by surfing acceleration [7].

To understand what determines the differences in the wave saturation and collapse for the Vlasov and for the PIC simulations we compare the electron phase space distributions for cases 2 and 3. In Fig. 3 we show the electron density as a function of the position. Both simulations show practically identical density modulations for the same electric field amplitude.

Figure 4 shows the spatially averaged electron distributions corresponding to Fig. 3 and normalized to their peak initial value. The electron phase space distribution in the interval $-10 < v' < 30$ is well represented by the Vlasov simulation. In contrast, the electrons in the PIC simulation are well represented only for $|v'| < 10$. The island of trapped electrons centered around $\hat{v}_{b1} = 15$ is just beginning to develop in the PIC simulation while it is fully developed in the Vlasov simulation.

The Vlasov simulation can represent a Maxwellian velocity distribution for the electrons in the interval $\pm 8 v_{\mathrm{th},e}$ compared to the interval $\pm 3 v_{\mathrm{th},e}$ for the PIC simulation, both in the frame of reference where the electron mean speed vanishes. Since the velocity gap between ω_u/k_u and the maximum velocity reached by thermal electrons is less in the Vlasov simulation, the waves interact with the electrons at a lower E. The trapped particle island develops at lower amplitudes causing the wave to saturate earlier in the Vlasov simulation than in the PIC simulation which is observed in Fig. 2. This is further confirmed by the observation that the peak amplitude of curve 1 in Fig. 2 is higher than that of curve 2 because its larger $\hat{v}_{b1}$ gives a larger velocity gap between the fastest electrons and ω_u/k_u.

The peak amplitude for curve 3 is identical to that in [8] and it exceeds that of curves 1 and 2. This implies by $v_T^2 \sim E$ a larger trapped particle island in the PIC simulation than in the Vlasov simulations pushing the plasma into a different nonlinear regime. This is likely to be the reason for their differing stability. A detailed investigation of this issue is left to future work.

Once the BGK wave collapses, its energy is transferred to the electrons further accelerating them. In Fig. 5 we show the electron velocity distributions for cases 2 and 3 at $t' = 280\pi$. Both distributions are similar despite the different lifetimes of the BGK modes and the electrons cover the speed interval between $\pm 4 v'_{b1}$ which is in line with previous results [6–8].

In summary we have compared the evolution of a proton beam driven wave in a PIC and in a Vlasov simulation. Our initial parameters and our interpretation of the results best represent a thermalized upstream plasma without a significant hot electron component at the time the wave interacts first with the electrons. Our beam parameters have been chosen such as to minimize computation times. We leave the investigation of how our results are modified by the presence of a hot electron population and by other beam parameters to future work.

We have identified differences between results computed by both simulation codes with a significant bearing for electron injection at SNR shocks. These differences

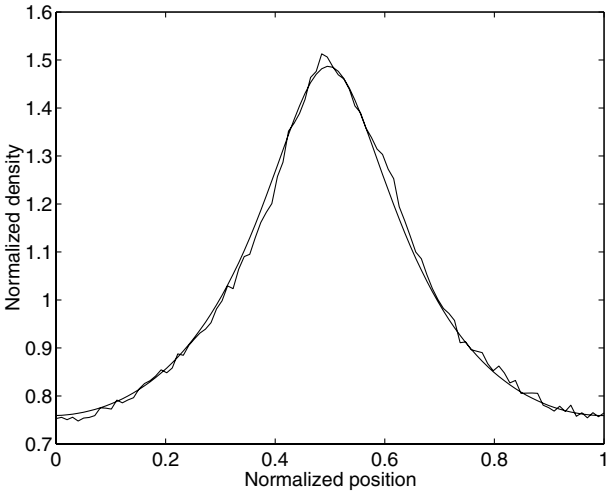

FIG. 3. The electron densities for cases 2 and 3 at the time $E/E_c = 0.56$ are reached first. Both curves are practically identical showing that for this electric field amplitude both electron distributions are in the same nonlinear regime. We show one out of four wave periods in our simulation box. The other three periods show an equally good agreement.

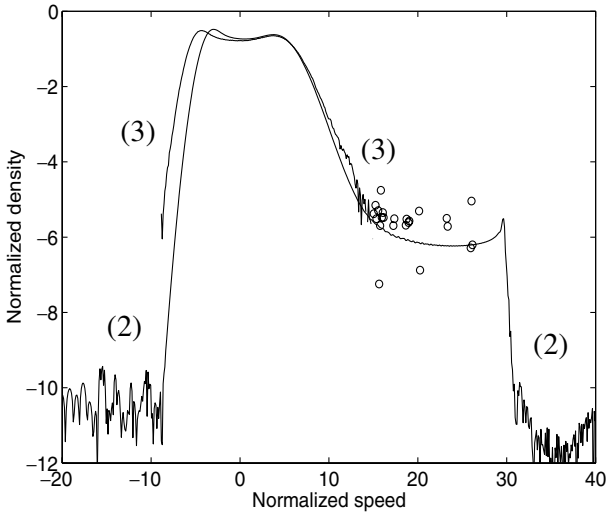

FIG. 4. The spatially averaged $\log_{10}(f_e(v'))$ for cases 2 and 3 for $E/E_c = 0.56$. The Vlasov simulation shows a well-defined trapped particle island with a maximum speed $v' = 30$. The PIC simulation shows a fluctuating electron density at high speeds (circles). Both codes show a qualitatively similar distribution for the untrapped electrons at lower v'.

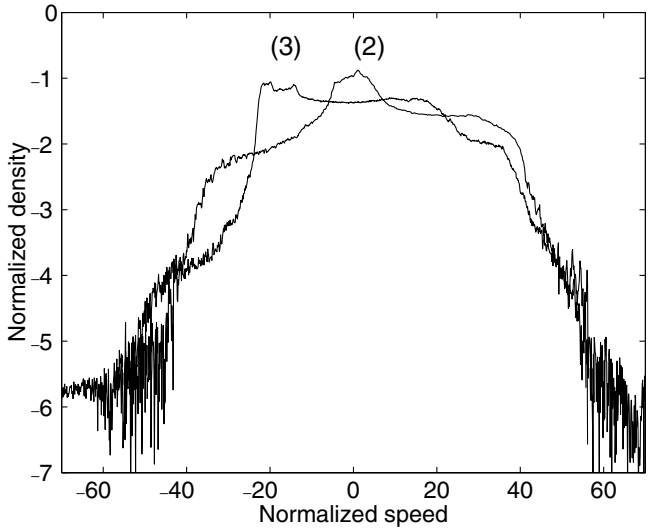

FIG. 5. The spatially averaged $\log_{10}(f_e(v'))$ at $t' = 280\pi$ for cases 2 and 3. After the BGK mode collapse the electrons cover the same velocity interval in phase space.

are most likely due to their different particle representations. The results obtained with the PIC simulation are in agreement with previous studies. The Vlasov simulations show, however, an increased lifetime of the BGK mode. At $\hat{v}'_{b1} = 15$ the lifetime of the BGK mode in the Vlasov simulation is comparable to that in [7] that excluded the sideband instability. We have to emphasize, however, that the BGK mode stability may be different in a two- or three-dimensional space. Above a critical beam speed $\hat{v}'_c \approx 20$ the Vlasov simulations show a rapid collapse of the BGK mode in line with PIC simulations.

Since our discussion based on Eqs. (1) and (2) is valid as long as all particle velocities involved are nonrelativistic we can obtain a simple estimate for $\hat{v}_c$ in the plasma in which the SNR shock is immersed. We obtain a lower bound by setting $v_{\mathrm{th},e}$ to the $v_{\mathrm{th},e} \approx 10^6$ m/s of the cool 10^1 eV ISM electron component. We obtain an upper bound by taking the thermal velocity of the hot 10^2 eV ISM population of $v_{\mathrm{th},e} \approx 4 \times 10^6$ m/s. We may thus expect that $0.06c < \hat{v}_c < 0.26c$.

Below $\hat{v}_c$ the Vlasov simulations show a stable BGK mode implying that electrons may be accelerated by the surfing mechanism. Here, the collapsing wave is in most cases not able to accelerate electrons to energies of 10^5 eV and above required for injection. This strongly suggests surfing acceleration to be the injection mechanism at slow SNR shocks. Above $\hat{v}_c$ the injection mechanism is likely to be electron acceleration due to the wave collapse since here the PIC code and the Vlasov code predict a lifetime of the BGK mode that is too short to significantly accelerate electrons by surfing acceleration. Since however the collapsing wave can accelerate electrons up to a maximum speed of $4\hat{v}_{b1}$ it could provide the seed electrons for Fermi acceleration if the shock and thus the shock-reflected ion beam have a speed comparable to or exceeding $0.2c$ such as SN1998bw [17].

This work has been supported by the Swedish National Supercomputer Centre (NSC), by the Swedish research council NFR (Contract No. 25420402), through the German Sonderforschungsbereich 591, by Linköpings University, and by the European Commission (Contract No. HPRN-CT-2001-00314). We are indebted to Professor Padma Shukla for his suggestions and for his help in putting together this article.

*Electronic address: mardi@itn.liu.se
†Electronic address: bengt@tp4.rub.de
‡Electronic address: andreas@cs.wm.edu
§Electronic address: andyn@itn.liu.se

[1] S. P. Reynolds, Space Sci. Rev. **99**, 177 (2001).
[2] P. L. Biermann and J. P. Cassinelli, Astron. Astrophys. **277**, 691 (1993).
[3] A. R. Bell, Mon. Not. R. Astron. Soc. **182**, 147 (1978).
[4] E. Berezhko, Space Sci. Rev. **99**, 295 (2001).
[5] R. A. Treumann and T. Terasawa, Space Sci. Rev. **99**, 135 (2001).
[6] M. E. Dieckmann *et al.*, Astron. Astrophys. **356**, 377 (2000).
[7] K. G. McClements *et al.*, Phys. Rev. Lett. **87**, 255002 (2001).
[8] M. E. Dieckmann *et al.*, Phys. Plasmas **7**, 5171 (2000).
[9] H. Schmitz, S. C. Chapman, and R. O. Dendy, Astrophys. J. **579**, 327 (2002).
[10] M. Hoshino and N. Shimada, Astrophys. J. **572**, 880 (2002).
[11] H. Schmitz, S. C. Chapman, and R. O. Dendy, Astrophys. J. **570**, 637 (2002).
[12] N. Shimada and M. Hoshino, Phys. Plasmas **10**, 1113 (2003).
[13] I. B. Bernstein, J. M. Greene, and M. D. Kruskal, Phys. Rev. **108**, 546 (1957).
[14] J. W. Eastwood, Comput. Phys. Commun. **64**, 252 (1991).
[15] B. Eliasson, J. Sci. Comput. **16**, 1 (2001).
[16] B. Eliasson, J. Comput. Phys. **181**, 98 (2002).
[17] S. R. Kulkarni *et al.*, Nature (London) **395**, 663 (1998).